

# Evaluation of Power Harvesting on DC–DC Converters to Extract the Maximum Power Output from TEGs Arrays under Mismatching Conditions

D. Sanin-Villa<sup>1,\*</sup>, E. Henao-Bravo<sup>1</sup>, C. Ramos-Paja<sup>2</sup>, and F. Chejne<sup>2</sup>

<sup>1</sup>Instituto Tecnológico Metropolitano, Cra. 74d #732, Medellín, Colombia.

<sup>2</sup>Universidad Nacional de Colombia, Av. 80 #65–223, Medellín, Colombia.

**Abstract**— Thermoelectric generators (TEGs) can transform wasted heat from industrial processes into electrical power. The power provided by TEGs systems depend on the temperature gradient, where an ideal situation for the TEGs operation is when all the modules of an array are exposed to the same temperature difference. Unfortunately, that condition is not always possible since the TEG arrays are exposed to non-uniform thermal conditions (known as mismatching). This paper proposes a novel equivalent model to represent the electrical behavior of a TEG, including a high-order approximation for the temperature dependence properties of the internal resistance and output voltage. Several configurations proposed to mitigate the mismatching phenomenon on TEGs arrays were tested, which are based on boost converters, PI controllers and the perturb and observe algorithm for maximum power point tracking: 1) TEGs serial connection with a single power converter, 2) a parallel connection where each TEG has its own converter, and 3) a serial connection where each TEG has its own converter. Those tests were performed in three temperature differences (50°C, 100°C and 180°C) to study the impact of the mismatching thermal condition over the total output power. The maximum power delivered by the traditional case 1 was 10.7 W; while the output power provided by case 2 was 12.07 W (12.8 % higher) and 11.1 W (3.7 %) for case 3.

**Keywords**— Mismatching conditions, Power converters, Thermoelectric systems.

## 1. INTRODUCTION

The world growing energy demand has contributed to several concerns regarding the rational and efficient use of energy resources. With the Paris agreements signed in 2015, some countries pledged to decrease the global warming rate by the end of the '30s [1], and that objective can be achieved by taking a series of actions focused on energy efficiency, reduction of CO<sub>2</sub> emissions, and the use of renewable energy [2]. Thermoelectric generators (TEG) are solid-state semiconductor devices that directly convert the temperature gradient between two surfaces into electrical energy [3]. The most attractive advantages of this technology is the lack of mobile parts, lower maintenance, and lower acoustic contamination compared with other thermal machines. In recent years, thanks to the lower manufacturing cost and the development of new materials with higher conversion rates, TEG devices have been used in different contexts as thermoelectric solar generation systems [4], [5], thermal energy harvesting for IoT devices and wearables [6], hybrid photovoltaic-TEG systems [7], [8], waste heat recovery from exhaust gas applications [9], small scale geothermal sources [10], and even in space exploration with radioisotope heat fuel application like the last rover send by NASA in the Mars Mission Perseverance, among others [11].

### 1.1. Maximum power point in generation systems

The analysis of thermoelectric generation systems also requires to model the power converter interfacing the generator and the electrical load. Mathematical models enables to predict the performance of a TEG system and supports the development of efficient designs and control systems. To extract the maximum power from the TEG array, it is necessary to reach the maximum power point (MPP) of the whole system using DC-DC power converters and a maximum power point tracking algorithm (MPPT). Standard algorithms for MPPT have been studied and reported for TEG systems: according to [12], to maximize the power produced by the TEG, the electrical load impedance should be equal to the TEG's internal resistance. The open-circuit voltage (OCV) is the most used MPPT method for TEGs, where the maximum extraction power is reached by considering the linear relation between the output voltage and current for TEGs [12], and the MPP is located by fixing the load voltage at half of the output open voltage [14]. Other methods have been originally developed for PV systems, where a nonlinear relationship between the voltage and current is presented. In the perturb and observe method (P&O), the operating point is perturbed, and the power output response is observed to decide the direction of the following perturbation to reach a maximum power [15]. Similarly, the incremental conductance (INC) finds the MPP by comparing the instantaneous conductance to the incremental derivative conductance [16]. Complex techniques such as the adaptive rapid neural optimization (ARNO) approach have also been studied recently [17]. Novel methodologies, such as the machine learning-based MPPT technique, have been used to harvest the maximum power of a centralized TEG system under various operating conditions [18]. In addition, the fast atom search optimization method was used to approximate the global maximum power point [19], [20], and control methods for regulating proportional load sharing [21] have been also developed.

Received: 25 Jul. 2022

Revised: 10 Dec. 2022

Accepted: 12 Jan. 2023

\* Corresponding author:

E-mail: danielsanin@itm.edu.co (D. Sanin-Villa)

DOI: 10.22098/JOAPE.2023.11207.1836

Research Paper

© 2023 University of Mohaghegh Ardabili. All rights reserved

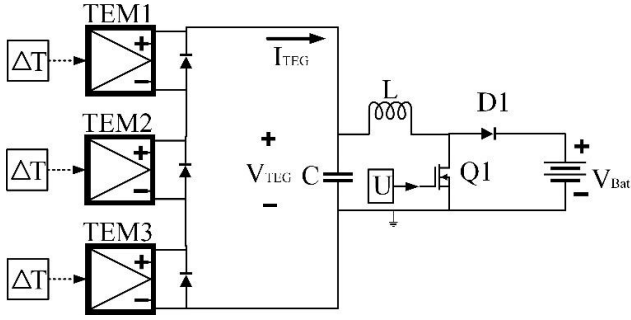


Fig. 1. Serial TEG array with a single boost converter

## 1.2. The mismatching thermal conditions

The power provided by TEG systems depends on the temperature gradient, where an ideal situation is when all the modules of an array are exposed to the same temperature gradient. Unfortunately, the TEG arrays are usually exposed to different thermal conditions. Other situations like the lack of maintenance, dust, and non-uniform heat sources could cause different temperature conditions between the modules. This is known as mismatching conditions, and the main consequence is the difference in power output generated by each module inside the array. Possible solutions are to connect each TEG with one local converter or set up different TEGs over an isothermal area and cluster the TEGs with equal thermal gradients into a single array [22].

A single power converter can be used for combinations of TEGs connected in serial and/or parallel structures [23]. Yang et al. proposed an adaptive compass search for maximum power point tracking (MPPT) of a centralized thermoelectric generation (TEG) system under non-uniform temperature conditions [24], but such a work is based on a simple model for the thermoelectric cell formulated from [25]. That model assumes a mean value for the Seebeck coefficient and no variable properties for the thermoelectric materials. Fig. 1 shows the classical connection used to extract the maximum power output from TEG systems [17, 26, 27], but there are also a few works where individual converters are designed for each TEG module.

Modeling TEG systems under mismatching thermal conditions is a challenging task, this mainly because the non-uniform thermal distributions cause multiple operative conditions for each TEG module. Thus, each module has a particular electrical characteristic curve for the specific temperature gradient, and the total configuration curve must be computed from the individual modules behavior at the array operation conditions. Therefore, multiple MPP local peaks could appear with only one global MPP. In this work, a novel equivalent model to represent the electrical behavior of a TEG array with high order approximation for the temperature dependence properties will be presented; also, different topologies for DC-DC converters connection are evaluated, those aimed at extracting the maximum power output from the TEG array under mismatching conditions. In addition, the effect of mismatching thermal conditions and the conversion efficiency on thermoelectric power generation for both classical and distributed configurations are also analyzed.

The rest of the paper is organized as follows: Section 2 reports the design and models of both the TEG and the boost converter; Section 3 presents a comparison and detailed analysis of different configurations of the TEG array to operate under mismatching conditions. Finally, the conclusions of the work are presented in Section 4.

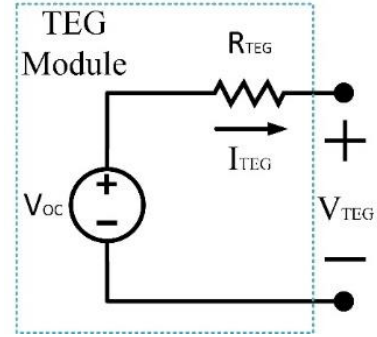


Fig. 2. TEG circuitual representation

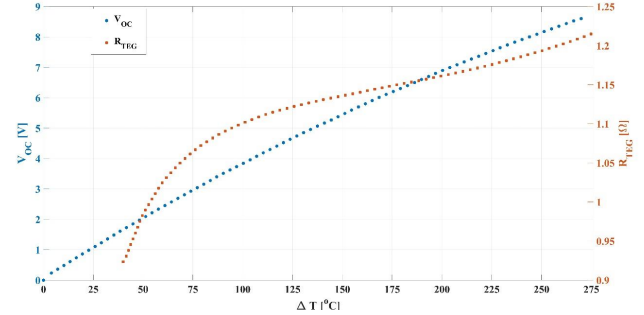


Fig. 3. Open-circuit voltage and internal resistance of the TEG module

## 2. MATERIALS AND METHODS

### 2.1. TEG circuitual model

For this study, a circuitual representation based on a nonlinear model of a commercial thermoelectric generator is built using the TEG TEG1-12611-6.0 produced by TEC TEG MFR [23]. Fig. 2 shows a typical Thevenin equivalent model of a TEG module formed by an open-circuit voltage source ( $V_{OC}$ ) and the internal resistance of the module ( $R_{TEG}$ ):

The voltage induced by the TEG is related to the temperature difference according to the following relationship [28]:

$$V_{OC} = \alpha(T) \Delta T \quad (1)$$

In the previous expression  $\alpha$  is the Seebeck coefficient and  $\Delta T$  is the difference between the hot ( $T_h$ ) and cold ( $T_L$ ) side of the TEG module. In many studies,  $\alpha$  in (1) is assumed to be constant, and it is considered an effective property. However, this assumption yields to ignore a rejection heat caused by the Thomson effect ( $\tau$ ) defined by (2) [29]:

$$\tau = T \frac{d\alpha}{dT} \quad (2)$$

From the TEG datasheet, the experimental values for  $V_{OC}$  and  $R_{TEG}$  as a function of  $\Delta T$  are extracted for a constant temperature in the cold side  $T_L = 30^\circ\text{C}$ ; Fig. 3 shows both functions. Those functions represent the TEG's actual behavior, including the influence of the temperature over the thermoelectric material properties.

The voltage dataset is fitted to the second-order function given in (3), and the internal resistance is fitted to the fourth-order expression given in (4) with a square correlation coefficient of  $R^2 = 1$  and  $R^2 = 0.99$ , respectively. The parameters in equations (3) and (4) are:  $\{a = -4 \times 10^{-5}, b = 0.0413, c = 0.0631\}$  and  $\{d = -4 \times 10^{-10}, e = 3 \times 10^{-7}, f = -9 \times 10^{-5}, g = 0.0112, h = 0.6095\}$ , respectively.

$$V_{oc} = a\Delta T^2 + b\Delta T + c \quad (3)$$

$$R_{TEG} = d\Delta T^4 + e\Delta T^3 + f\Delta T^2 + g\Delta T + h \quad (4)$$

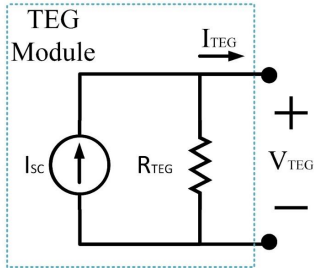
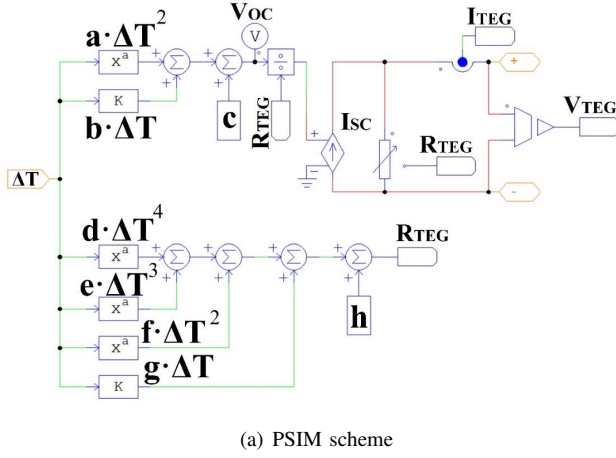


Fig. 4. Circuit representation of TEG module considering thermal conditions

$$I_{sc} = V_{oc}/R_{TEG} \quad (5)$$

Considering Equations (3) and (4), a circuit model for the TEG is designed on the circuit simulation software PSIM as presented in Fig. 4(a). The circuit consists of a current source ( $I_{sc}$ ), calculated as given in (5), in parallel with the equivalent resistance ( $R_{TEG}$ ); this representation is a Norton equivalent (Fig. 4(b)) of the classical TEG representation shown in Fig. 2. Therefore, this model considers the effect of the temperature on the thermoelectrical properties in a wide range of thermal conditions (up to  $\Delta T = 280^\circ C$ ). Based on the previous detailed circuit model for the TEG module, the characteristic operative curves power vs. voltage ( $P$  vs  $V$ ) and current vs. voltage ( $I$  vs  $V$ ) for three different  $\Delta T$  values ( $50^\circ C$ ,  $100^\circ C$  and  $180^\circ C$ ) are generated and presented in Fig. 5(a). In such a figure the curved lines represent the power and the straight lines the current for different voltages. Fig. 5(a) shows the power, current, and voltage at MPP for three TEG modules, each one operating at a different  $\Delta T$  value. The module operating at  $\Delta T = 180^\circ$  delivers 9.25 [W] at the MPP with 2.99 [A] and 3.087 [V]. For the TEG operating at  $\Delta T = 100^\circ$  the power at MPP is 3.3 [W], the current is 1.727 [A] and the voltage is 1.911 [V]. Finally, the TEG operating at  $\Delta T = 50^\circ$  delivers 1.049 [W] at the MPP with 1.0414 [A] and 1.008 [V]. Therefore, to reach the MPP it is necessary to modify the operating voltage when  $\Delta T$  changes.

On the other hand, if each TEG module operates at the individual MPP, the total power ( $P_T$ ) is obtained by the following expression:

$$P_T = \sum_{i=1}^n P_i \quad (6)$$

where  $P_i$  are the individual MPP power of each module at its respective temperature gradient; in this example  $P_T = 13.6W$ . In renewable energy applications, like thermoelectric generators, it is common to find a series connection of the TEG modules, but

the mismatching effect can reduce the harvested power. In this way, Fig. 5(b) shows the power vs. voltage characteristic curve for the three TEG modules operating in mismatching conditions ( $\Delta T$  values of  $50^\circ C$ ,  $100^\circ C$  and  $180^\circ C$ ): the figure shows the global MPP (11.73W), which is 15.94% lower than the sum of all individual MPPs (13.6W). This is due to the mismatching condition prevents that each module operates in its individual MPP. Moreover, there is a local maximum at 11.625W; therefore, an MPPT can be trapped in a suboptimal maximum, thus producing even less power.

Based on the previous analyses, it is necessary to use power converters to isolate the operation of each TEG module, thus enabling the operation at the MPP conditions shown in Fig. 5(a). However, it is also necessary for an MPPT to look for the MPP in each temperature condition for each TEG module.

## 2.2. Boost converter

For practical applications, the voltage of TEG systems must be driven by a power converter, which interfaces the power source with the load. Then, a traditional boost DC-DC device is designed to provide the voltage level required by the load, and the same time, to impose the desired voltage level to the TEG. Fig. 6 shows the circuit structure of the proposed boost converter, which is formed by a Mosfet switch ( $Q_1$ ) driven by a PWM signal and a PI controller, one diode ( $D_1$ ), a capacitor (C), and an inductor (L).

To design the power converter, the energy storage elements C and L must be selected to be able to manage the maximum power delivered by the interconnected TEGs and to reduce the current and voltage ripples on the TEG.

The voltage ripple in the capacitor ( $\Delta_v$ ) represents the voltage oscillation around the operating voltage of  $V_{TEG}$ , hence the TEG module exhibits a power ripple ( $\Delta_p$ ) affecting the overall power production. Therefore,  $\Delta_v$  must be selected to ensure an acceptable  $\Delta_p$  around the operating power point. Such a voltage ripple limit is obtained from (7), which relates the voltage and power in a resistive circuit, thus it is applicable to the Norton equivalent shown in Fig. 4(b).

In the same way, the current ripple in the inductor ( $\Delta_i$ ) must fulfill the power ripple parameter given in (8), which is the classical relationship between electrical power, current and voltage. The power ripple must be selected lower than 1% of the MPP power to limit the power losses.

The calculation of both passive elements, L and C, is performed using the steady-state analysis presented in [30], which provides the small-signal equations (9) and (10) for the inductor current ripple and capacitor voltage ripple in the two-pole filter of a boost converter. For the L and C calculation,  $V_{TEG}$  and  $R_{TEG}$  are selected from the TEG datasheet at the MPP, and the switching period ( $T_s$ ) is selected to impose a switching frequency ( $F_s$ ) higher than 50kHz, as recommended in [30].

$$\Delta_v = (\Delta_p R_{TEG})^{\frac{1}{2}} \quad (7)$$

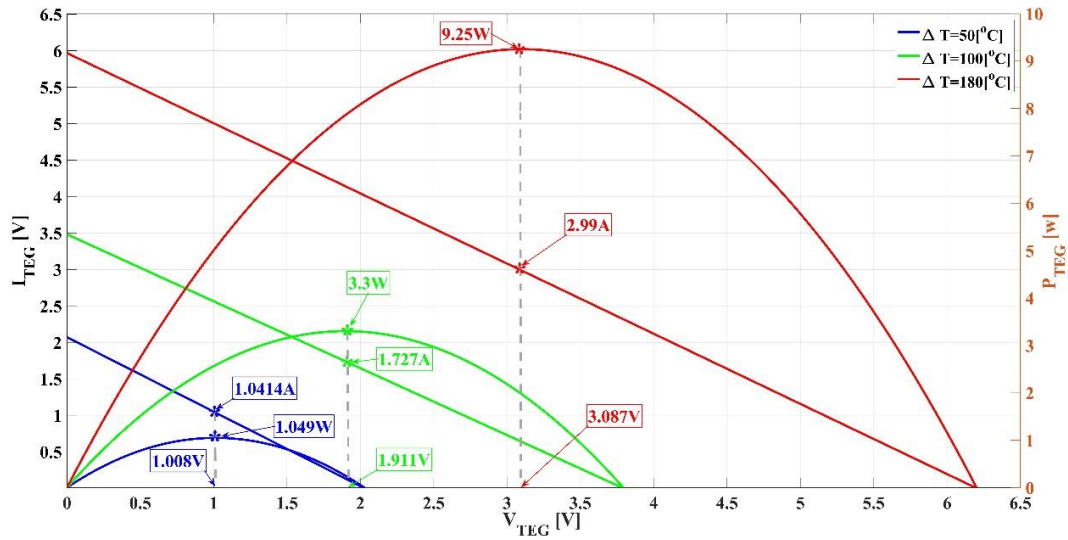
$$\Delta_i = \Delta_p / \Delta_v \quad (8)$$

$$L = V_{TEG} T_s / 2 \Delta_i \quad (9)$$

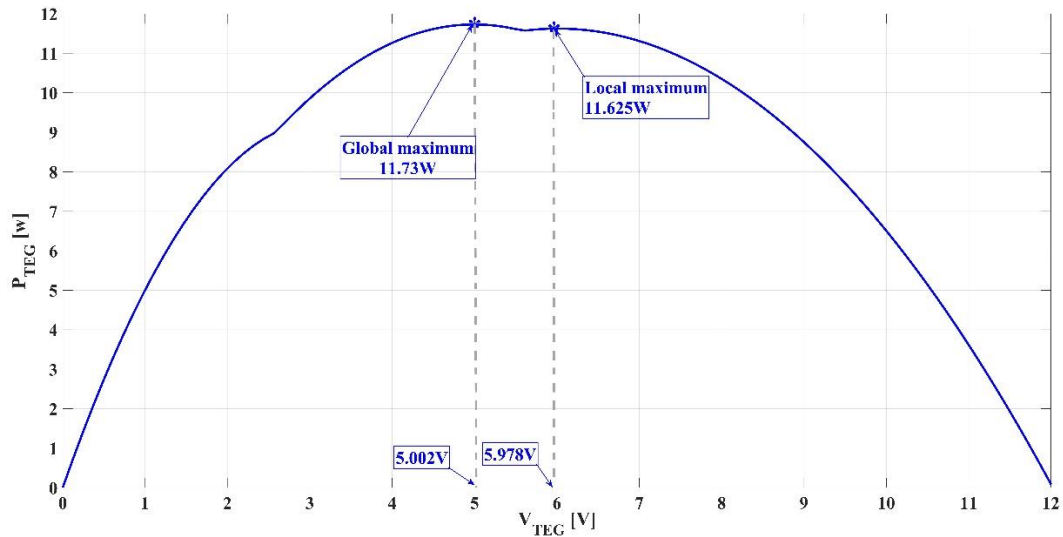
$$C = V_{TEG} T_s^2 / 16 \Delta_v L \quad (10)$$

Fig. 6 shows a boost converter interfacing a TEG module to extract the power and store it in a battery. This system is regulated by a PID controller and a MPPT P&O algorithm.

As discussed in subsection 2.1, the power converter is required to regulate the operating voltage  $V_{TEG}$  of the TEG in agreement with the MPP condition, but when  $\Delta T$  changes also the MPP value of  $V_{TEG}$  changes. Therefore, the MPPT algorithm (P&O) tracks the optimal  $V_{TEG}$  value, which is imposed as the reference  $V_{REF}$  to a voltage controller. In this work the TEG module is regulated using a PID controller, which defines the duty cycle reaching the PWM driving the transistor Q1 of the boost converter.



(a) Individual power and current curves at three different  $\Delta T$



(b) Power vs. current for a series array of three cells with different  $\Delta T$

Fig. 5. Power and current curves for different temperature gradients

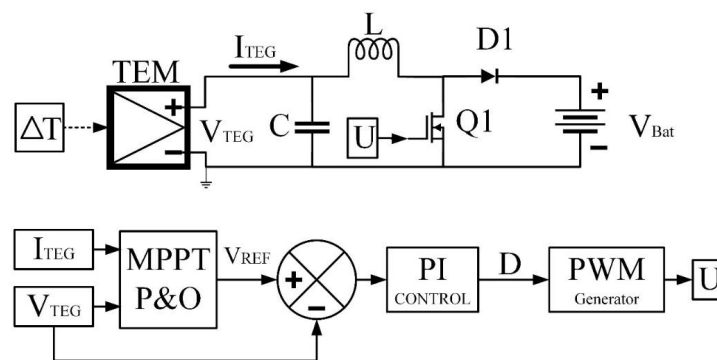


Fig. 6. DC-DC boost converter

A proper design of the PID controller must be based on the dynamic behavior of the system formed by both the TEG module and the boost converter. Therefore, the following subsection develops the modeling of the system and the controller design.

### 2.3. Dynamic model of the TEG power system

The dynamic behavior of the TEG/converter circuit is described using the differential equations (11) and (12), which were obtained using the flux and charge balances in the power circuit as it is described in [30].

$$\frac{dV_{TEG}}{dt} = -\frac{1}{C} \left( i_L - I_{sc} + \frac{V_{TEG}}{R_{TEG}} \right) \quad (11)$$

$$\frac{di_L}{dt} = \frac{1}{L} (V_{TEG} + V_{Bat} (D - 1)) \quad (12)$$

The previous dynamic equations can be expressed as presented in (13), where the state variables ( $x$ ) are capacitor voltage ( $V_{TEG}$ ) and inductor current ( $i_L$ ).

$$\dot{x} = \begin{bmatrix} \dot{V}_{TEG} \\ \dot{i}_L \end{bmatrix} = \begin{bmatrix} -\frac{i_L - I_{sc} + \frac{V_{TEG}}{R_{TEG}}}{C} \\ \frac{V_{TEG} + V_{Bat}(D-1)}{L} \end{bmatrix} \quad (13)$$

This second-order system is linearized around an operating point to find the transfer function, which relates the state variables with the control variable  $D$  (duty cycle of the PWM signal). For this model, the input array ( $U$ ) corresponds to the system inputs: short-circuit current of the TEG ( $I_{sc}$ ), battery voltage ( $V_{Bat}$ ) and the control input ( $D$ ). The Jacobian matrices of  $\dot{x}$  relative to  $x$  ( $A$ ) and  $U$  ( $B$ ) are calculated as shown in (14):

$$A = \begin{bmatrix} -\frac{1}{CR_{TEG}} & -\frac{1}{C} \\ \frac{1}{L} & 0 \end{bmatrix}; B = \begin{bmatrix} \frac{1}{C} & 0 & 0 \\ 0 & \frac{D-1}{L} & \frac{V_{Bat}}{L} \end{bmatrix} \quad (14)$$

To define the transfer function needed to find the Jacobian matrices of the output variable ( $Y = V_{TEG}$ ) with respect to the state vector  $x$  and input variables  $U$ , two additional matrices are defined:  $C_s = [1 \ 0]$  and  $D_s = [0 \ 0 \ 0]$ . Then, the transfer function  $H(s)$  between the TEG voltage ( $V_{TEG}$ ) and the duty cycle is the following one:

$$H(s) = \frac{Ls + D' - V_{Bat}}{CLs^2 + \frac{L}{R}s + 1} \quad (15)$$

### 2.4. The MPPT algorithm

Due to the nonlinear behavior of the TEG module and the constantly changing environmental conditions, it is not possible to find a unique offline MPP. Therefore, the MPPT defines a voltage reference for the PI controller, which sets the duty cycle for the PWM signal driving the Mosfet [31]. In this work, the Perturb and Observe (P&O) algorithm has been implemented due to its simplicity, fast response, low cost, and commercial use [20]. The P&O method perturbs the operating voltage of the TEG and the power output is measured; if the power is decreased, the voltage imposed to the TEG is perturbed in the opposite direction; otherwise, the voltage is perturbed in the same direction. Two parameters must be defined for this algorithm: the perturbation voltage and the perturbation period. The selection of those values must be considered that high  $\Delta V$  values produce faster responses, and those must be large enough to produce a measurable power perturbation (higher than the power ripple). Long perturbation periods ( $T_a$ ) produce a slow response; therefore, small values are recommended. Finally, the work reported in [33] demonstrated that  $T_a$  must be larger than the settling time of the source voltage to ensure the stability of the P&O algorithm.

## 3. RESULTS AND DISCUSSION

Several TEG modules can be connected in parallel or series configuration, which allows the system to produce higher output power. When the temperature difference of each thermoelectric module is different, the mismatching condition increases de power losses as it is discussed in [34]. To extract the maximum power from each TEG module in the array, the following configurations are proposed:

- 1) DMMPT series: each module is interfaced using a single power converter with MPPT control; and the output of the converters are connected in series to provide an additional boosting factor. Therefore, the voltage gain for each converter is low, thus introducing small power losses under mismatching conditions. In this structure the sum of converters' output voltages is equal to the battery voltage ( $V_{Bat}$ ), hence the behavior of each module voltage is affected by the changes on the other TEG modules in the series connection.
- 2) DMMPT in parallel: each TEG module reaches its MPP with an individual power converter, but in this case the converters' outputs are connected in parallel. For this configuration, the output voltage must be the same for all the power converters, and every module works independently at its own MPP. One of the advantages of this structure, in comparison with the centralized MPPT techniques, is the ability to support plug-and-play systems, where each module can be removed or connected from the battery without compromising the performance of the other TEG modules.

This section presents the results of the MPPT design of the centralized TEG system (Fig. 1) and a detailed analysis of the DMPPT solutions. Fig. 6 shows the DMPPT configurations in a) parallel and b) series connection.

The evaluation of the DMPPT solutions is based on the simulation of the systems reported in Figures 1 and 6, those considering DC-DC boost converters designed with the following parameters:  $\Delta_p = 0.1\%P_{MPP}$ ,  $P_{MPP} = 3.3W$ ,  $F_S = 100 \text{ kHz}$ ,  $L = 220 \mu H$  with an internal resistance of  $36.45 \mu\Omega$ ,  $C = 1.14 \mu F$ ; and the P&O is set to  $\Delta V = 0.2V$  and  $T_a = 5 \text{ ms}$ . Finally, the PI controller was designed from the plant model  $H(s)$  using the pole-placement technique, obtaining the PI parameters  $K_p = -19.2 \mu V^{-1}$  y  $\tau_I = 34.92 \text{ ns}$  (integral time).

### 3.1. Classical TEG array with a single boost converter

Fig. 7 and Table 1 show the results of three TEG modules connected in series and interfaced with a single boost converter. The sum of the individual power produced by each TEG module ( $P_B = 13.59W$ ) is higher than the power produced by the array (11.73 W), which is caused by the mismatching condition and the efficiency of the boost converter. The total voltage of the array is the sum of individual modules voltages, and it is exceptionally close to the MPP voltage in Fig. 5(b). In this solution, the current is the same for all the TEG modules and equal to 2.392 A.

For the current working point, it is observed in Fig. 5(a) that the  $TEG_2$  works near its MPP, while  $TEG_1$  operates on the right side of the power curve, and  $TEG_3$  is working on the left side. When the TEG module works at the right side, with a current value higher than the MPP, the Peltier effect increases and cause a variety of temperatures on the cold and hot side of the module, reducing the efficiency. Instead, when it works at the left side, lower current flows through the TEG and the thermal conductivity decrease, thus causing more significant temperature difference between the hot and cold side of the TEG.

The simulation results of Fig. 7 show that the total array voltage follows the reference settled by the MPPT; and both the voltage ripple, and the average value, are over the reference point. In consequence, the power ripple is reflected on the battery. The power delivered to the battery is lower than the maximum power that could be provided by the TEG modules (11.7W): the battery receives 10.7W, which corresponds to an efficiency of

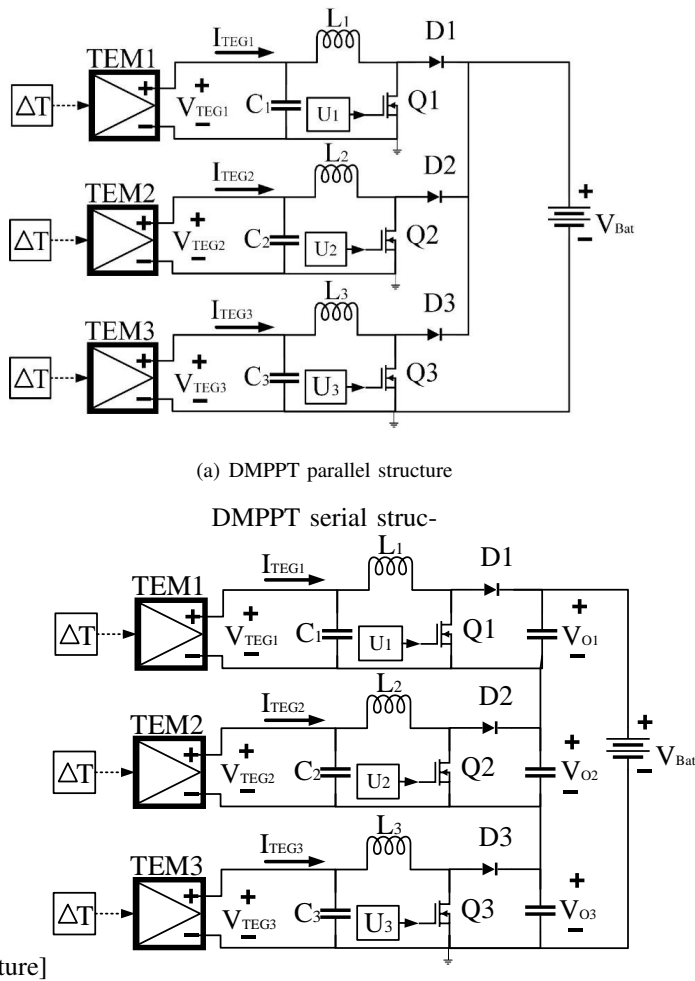


Fig. 7. Configurations proposed to mitigate the mismatching phenomenon

91.4%. Those results are explained by Fig. 5(b), since the global maximum is reached, but the maximum power of each cell is not achieved. Moreover, the converter efficiency also reduces the power delivered to the battery.

For the TEG module with lower temperature differential, the voltage and power delivered are zero, thus some power is missed. Finally, in this configuration the converter voltage gain is low, hence its efficiency is higher than 90%.

### 3.2. DMPPT parallel structure

Results of the three TEG converters connected in parallel are shown in Fig. 8, where the system reaches on average output power  $P_B = 12.07W$ . The power generated by each module, presented in Table 2, confirm that each TEG module works on its MPP, thus the overall power delivered to the load is 12.8% higher than in the previous (classical) case. Fig. 8 shows the voltage and power of the TEG with  $\Delta T = 180^\circ C$  (green line),  $\Delta T = 100^\circ C$  (blue line), and  $\Delta T = 50^\circ C$  (red line). The voltage of each module follows the reference value settled by the MPPT algorithms, and there is a voltage ripple that oscillates around the reference value; such a ripple is a consequence of the switching operation in the power converters.

The total power of the three TEG modules is, on average, 13.6W, which agrees with the information shown in Fig. 5(a). However, the total power delivered to the battery has an average value of 12.07W; therefore, the conversion efficiency of the boost converters, in this configuration, is 88.8%. Each module operates in

its corresponding MPP, and the parallel DMPPT solution manages to deliver more power to the battery than in the classical case, even if the converters' efficiency (88.8%) is lower than in the classical case (see Table 2).

### 3.3. DMPPT series structure

In this last case, the converters' outputs for each TEG are connected in series. Moreover, a  $200 \mu F$  capacitor at the output of the power converters was settled to establish the voltage and reduce output voltage ripple. Fig. 9 and Table 3 summarize the results of this arrangement, also reporting the voltage over each output capacitor. The average power delivered to the battery ( $P_B = 11.1W$ ) is also higher than in the classical configuration, but in this case the improvement is 3.7%.

The voltage, efficiency and total output power delivered by the series DMPPT configuration are presented in Fig. 9 for the three TEG modules under different temperature gradients. The magenta color shows the total power produced by the three cells, and the black trace reports the power delivered to the battery.  $TEG1$  and  $TEG2$  follow the MPPT settled by the control system and deliver their maximum power for each temperature difference (9.25W y 3.3W respectively), but the converter of  $TEG3$  can not delivered the maximum power (1.049W) even if the TEG is operating at the MPP. This is caused by the relation between the power delivered and the output voltage in each converter: since the converters are connectd in series, the output current is the same, thus the output voltage of each converter is proportional to the output power of the corresponding converter. Therefore, the higher the output power, the higher the output voltage. Moreover, this means that the converter delivering the highest power will also exhibits the higher voltage. However, since the total output voltage is fixed by the battery, the converter providing the lower power will also exhibit a very low output voltage, which could increase the power losses.

The previous phenomenon is observed in the simulations of Fig. 9: the higher output voltage will happen in the converter of  $TEG1$  when the maximum  $\Delta T$  occurs ( $\Delta T = 180^\circ C$ ,  $V_{O1} = 8.79V$ ), followed by the converter of  $TEG2$  ( $\Delta T = 100^\circ C$ ,  $V_{O1} = 2.75V$ ), and the last module ( $TEG3$ ) must supply the remaining value to achieve the battery voltage ( $V_{O3} = 0.456V$ ). The boost converter for  $TEG1$  and  $TEG2$  reach efficiencies of 87.7% and 77.3%, respectively, but the efficiency of  $TEG3$  is 40.7% due to power losses and the energy dissipated to achieve the output voltage imposed by the battery.

The conversion efficiency of this system averages 82%, which is the lowest efficiency in the three configurations; however, the power delivered to the battery is 11.1W, which is higher than the power provided by the classical configuration. Such a power conversion efficiency can be improved by using passive elements with lower ohmic resistance, which could also increase the cost. Another disadvantage of this configuration occurs when one TEG module changes the operation point, which also perturbs the other TEG modules, but a proper PI controller could regulate such a perturbation.

## 4. CONCLUSIONS

A new method to evaluate the TEG system was proposed according to the performance curve constructed with the manufacturer datasheet and the inclusion of maximum power point tracking algorithms. Also, different DC-DC converters connections were evaluated with aim of extracting the maximum power from TEG arrays operating under mismatching conditions. The maximum efficiency (91.4%) was reached by connecting the TEGs in series with a single boost converter, but none of the TEGs operate at their MPP, and the maximum power delivered to the battery was 10.7W. On DMPPT configurations, each thermoelectric module work at its MPP, but the conversion efficiency of the system is lower than in the classical case, with a maximum efficiency of 88.8% for the DMPPT parallel solution, and 82% in the case

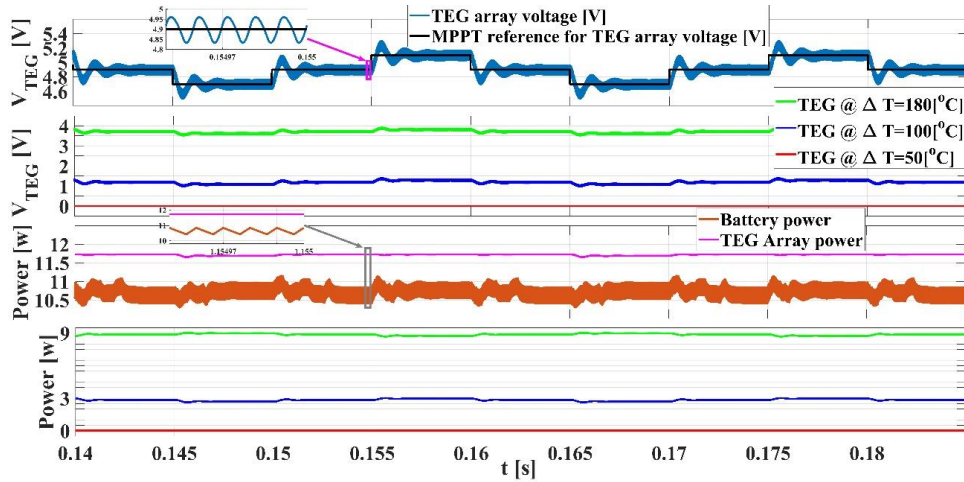


Fig. 8. Electrical parameters: serial configuration with a single boost

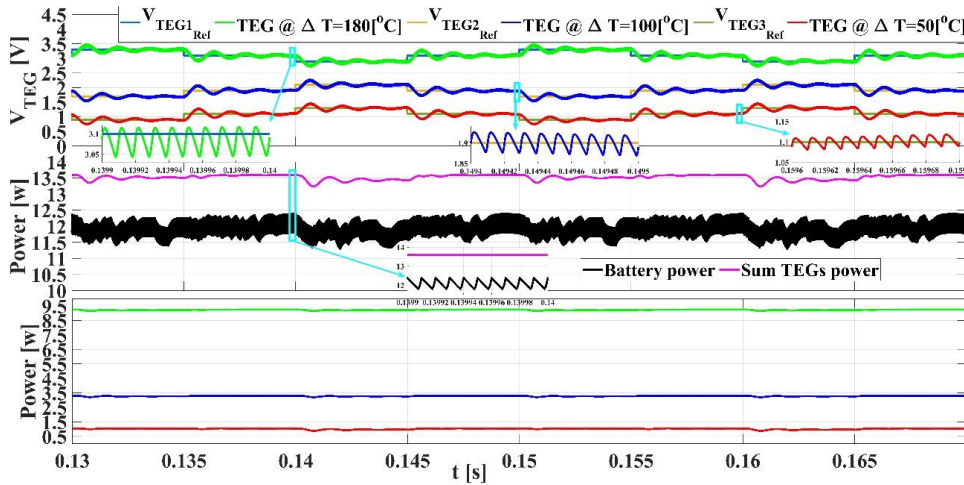


Fig. 9. Electrical parameters: parallel configuration with individual boost

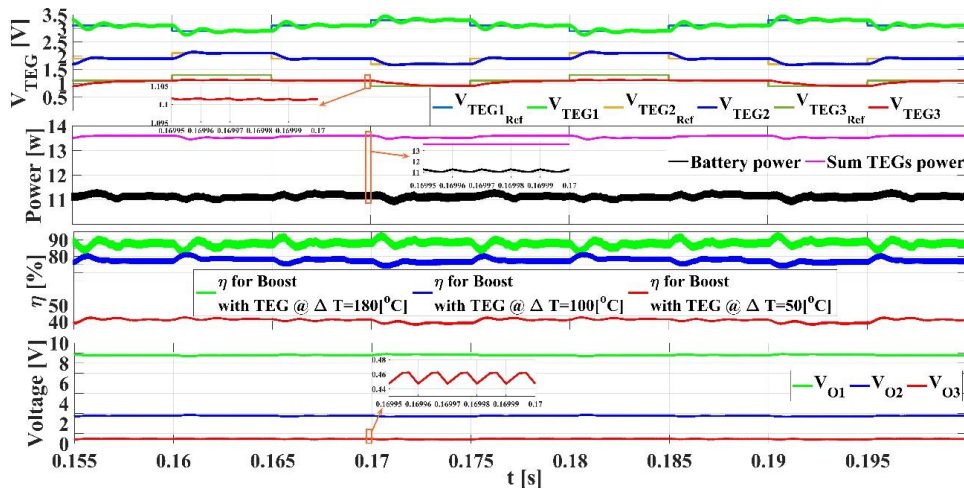


Fig. 10. Electrical parameters: serial configuration with individual boost

Table 1. Single boost converter for three TEG connected in series

Module	$\Delta T$ [ $^{\circ}C$ ]	$V_{TEG}$ [V]	$I_{TEG}$ [A]	$P_{TEG}$ [W]	$P_B$ [W]	$\eta_c$ [%]
$TEG_3$	50	0	2.392	0	10.7	91.4
$TEG_2$	100	1.186		2.837		
$TEG_1$	180	3.714		8.888		
<b>Total</b>		<b>4.9</b>		<b>11.725</b>		

Table 2. DMPPT parallel connection

Module	$\Delta T$ [ $^{\circ}C$ ]	$V_{TEG}$ [V]	$P_{TEG}$ [W]	$P_B$ [W]	$\eta_c$ [%]
$TEG_3$	50	1.1	1.04	12.07	88.8
$TEG_2$	100	1.89	3.3		
$TEG_1$	180	3.1	9.25		
<b>Total</b>			<b>13.6</b>		

Table 3. DMPPT serial connection

Module	$\Delta T$ [ $^{\circ}C$ ]	$V_{O1}$ [V]	$V_{TEG}$ [V]	$P_{TEG}$ [W]	$P_B$ [W]	$\eta_c$ [%]
$TEG_3$	50	0.456	1.055	1.04	11.1	82
$TEG_2$	100	2.749	1.899	3.3		
$TEG_1$	180	8.795	3.1	9.25		
<b>Total</b>		<b>12</b>	<b>5.7</b>	<b>13.6</b>		

where DMPPT series configuration. The power output delivered by the distributed structures always reached the MPP on each TEG, with a maximum power delivered to the battery of 11.1W and 12.07W for the DMPPT series and parallel, respectively. Therefore, this work confirms the improved power production of the DMPPT solutions over the classical centralized configuration. The higher losses in the DMPPT cases are explained by the significant number of elements in the converters that dissipate energy; nevertheless, the distributed array could be improved by selecting elements with lower parasitic resistances.

The P&O algorithm was used to optimize the power production, but it could be improved by adapting both perturbation period and amplitude according to the temperature differences. Similarly, an auto-tuning PI controller could be used to establish an adequate system response over more significant variations of temperature differences. Future works include evaluating the proposed method combined with new MPPT algorithms to assess the tracking speed, accuracy, and efficiency in TEG systems under mismatching thermal conditions.

## ACKNOWLEDGE

This work was supported by the Universidad Nacional de Colombia and Instituto Tecnológico Metropolitano. The authors want to thank the project “Estrategias para el desarrollo de sistemas energéticos sostenibles, confiables, eficientes y accesibles para el futuro de Colombia” funded by the call 890 of Minciencias, Contract number F RC 80740-178-2021-1 (Minciencias code 1150-852-70378, Hermes code 46771). The authors also thank the Alliance for Biomass and Sustainability Research–ABISURE–Universidad Nacional de Colombia, Hermes code 53024, for its support in the realization of this study.

## REFERENCES

- [1] UNFCC (United Nations Framework Convention on Climate Change), “Paris Agreement (Spanish),” p. 29, 2015, [Online]. Available: [http://unfccc.int/files/essential\\_background/convention/application/pdf/spanish\\_paris\\_agreement.pdf](http://unfccc.int/files/essential_background/convention/application/pdf/spanish_paris_agreement.pdf)
- [2] M. Morini, M. Pinelli, P. R. Spina, and M. Venturini, “Optimal allocation of thermal, electric and cooling loads among generation technologies in household applications,” *Appl. Energy*, vol. 112, pp. 205–214, 2013.
- [3] S. K. Bhukesh, A. Kumar, and S. K. Gaware, “Bismuth telluride (Bi2Te3) thermoelectric material as a transducer for solar energy application,” *Mater Today Proc.*, vol. 26, pp. 3131–3137, 2019.
- [4] M. Ge, Z. Wang, L. Liu, J. Zhao, and Y. Zhao, “Performance analysis of a solar thermoelectric generation (STEG) system with spray cooling,” *Energy Convers. Manage.*, vol. 177, pp. 661–670, 2018.
- [5] M. A. Qasim, V. I. Velkin, and A. K. Hassan, “Seebeck generators and their performance in generating electricity,” *J. Oper. Autom. Power Eng.*, vol. 10, no. 3, pp. 200–205, 2022.
- [6] A. Nozariasbmarz et al., “Review of wearable thermoelectric energy harvesting: From body temperature to electronic systems,” *Appl. Energy*, vol. 258, 2020.
- [7] E. Yin, Q. Li, and Y. Xuan, “Thermal resistance analysis and optimization of photovoltaic-thermoelectric hybrid system,” *Energy Convers. Manag.*, vol. 143, pp. 188–202, 2017.
- [8] R. Björk and K. K. Nielsen, “The performance of a combined solar photovoltaic (PV) and thermoelectric generator (TEG) system,” *Solar Energy*, vol. 120, pp. 187–194, 2015.
- [9] E. S. Mohamed, “Development and performance analysis of a TEG system using exhaust recovery for a light diesel vehicle with assessment of fuel economy and emissions,” *Appl. Therm. Eng.*, vol. 147, pp. 661–674, 2019.
- [10] R. ben Cheikh, B. el Badsı, and A. Masmoudi, “Geothermal sources-based thermoelectric power generation: An attempt to enhance the rural electrification in southern Tunisia,” in *2014 9<sup>th</sup> Int. Con. Ecol. Veh. Renewable Energies, EVER*, 2014.
- [11] A. Barco, R. M. Ambrosi, H. R. Williams, and K. Stephenson, “Radioisotope power systems in space missions: Overview of the safety aspects and recommendations for the European safety case,” *J. Space Saf. Eng.*, vol. 7, no. 2, pp. 137–149, 2020.
- [12] A. Belboula, R. Taleb, G. Bachir, and F. Chabni, “Comparative study of maximum power point tracking algorithms for thermoelectric generator,” *Lect. Notes Networks Syst.*, vol. 62, pp. 329–338, 2019.
- [13] A. Montecucco and A. R. Knox, “Maximum power point tracking converter based on the open-circuit voltage method

- for thermoelectric generators,” *IEEE Trans. Power Electron.*, vol. 30, no. 2, pp. 828–839, 2015.
- [14] S. Siouane, S. Jovanovic, and P. Poure, “Influence of contact thermal resistances on the open circuit voltage MPPT method for thermoelectric generators,” in *IEEE Int. Energy Conf., ENERGYCON*, 2016.
- [15] P. Shiriaev, K. Shishov, and A. Osipkov, “Electrical network of the automotive multi-sectional thermoelectric generator with MPPT based device usage,” *Mater Today Proc.*, vol. 8, pp. 642–651, 2019.
- [16] K. Bunthern, B. Long, G. Christophe, D. Bruno, and M. Pascal, “Modeling and tuning of MPPT controllers for a thermoelectric generator,” *2014 1<sup>st</sup> Int. Conf. Green Energy (ICGE)*, vol. 2, no. 3, pp. 220–226, 2014.
- [17] F. Li, D. Lin, T. Yu, J. Li, K. Wang, X. Zhang, B. Yang, and Y. Wu, “Adaptive rapid neural optimization: A data-driven approach to MPPT for centralized TEG systems,” *Electr. Power Syst. Res.*, vol. 199, p. 107426, 2021.
- [18] M. Hamza Zafar, N. Mujeeb Khan, M. Mansoor, and A. Khan, “Towards green energy for sustainable development: Machine learning based MPPT approach for thermoelectric generator,” *J. Clean Prod.*, vol. 351, p. 131591, 2022.
- [19] E. Naderi, S. J. Seyedshenava, and H. Shayeghi, “High gain DC/DC converter implemented with MPPT algorithm for DC microgrid system,” *J. Oper. Autom. Power Eng.*, vol. 11, no. 3, pp. 213–222, 2023.
- [20] B. Yang et al., “Fast atom search optimization based MPPT design of centralized thermoelectric generation system under heterogeneous temperature difference,” *J. Clean Prod.*, vol. 248, p. 119301, 2020.
- [21] R. Dadi, K. Meenakshy, and S. K. Damodaran, “A review on secondary control methods in DC microgrid,” *J. Oper. Autom. Power Eng.*, vol. 11, no. 2, pp. 105–112, 2023.
- [22] D. Sanin-Villa, O. D. Monsalve-Cifuentes, and E. E. Henao-Bravo, “Evaluation of thermoelectric generators under mismatching conditions,” *Energies*, vol. 14, Page 8016, vol. 14, no. 23, p. 8016, 2021.
- [23] M. TECTEG, “Specifications TEG Module TEG1-12611-6.0.” <https://thermoelectric-generator.com/>
- [24] B. Yang et al., “MPPT design of centralized thermoelectric generation system using adaptive compass search under non-uniform temperature distribution condition,” *Energy Convers. Manag.*, vol. 199, p. 111991, 2019.
- [25] Y. H. Liu, Y. H. Chiu, J. W. Huang, and S. C. Wang, “A novel maximum power point tracker for thermoelectric generation system,” *Renewable Energy*, vol. 97, pp. 306–318, 2016.
- [26] W. Zhu, X. Li, Y. Li, C. Xie, and Y. Shi, “Two-level energy harvesting strategy for multi-input thermoelectric energy system,” *Energy Reports*, vol. 8, pp. 4359–4372, 2022.
- [27] X. Liu, S. Yuan, Y. Zhou, B. Xu, W. Rong, Q. Li, X. Li, and P. Ma, “Theoretical and experimental research on control strategy of maximum power point tracking for monolayer thermoelectric generator considering the degree of disturbance,” *Energy Reports*, vol. 8, pp. 15124–15143, 2022.
- [28] S. Vostrikov, A. Somov, and P. Gotovtsev, “Low temperature gradient thermoelectric generator: Modelling and experimental verification,” *Appl. Energy*, vol. 255, 2019.
- [29] D. Sanin-Villa, O. D. Monsalve-Cifuentes, and E. E. Henao-Bravo, “Evaluation of Thermoelectric Generators under Mismatching Conditions,” *Energies*, vol. 14, p. 8016, vol. 14, no. 23, p. 8016, 2021.
- [30] R. W. Erikson and D. Maksimovic, *Fundamentals of Power Electronics Second Edition*, 1980.
- [31] B. Panda, A. Sarkar, B. Panda, and P. K. Hota, “A comparative study of PI and fuzzy controllers for solar powered DC-DC boost converter,” in *Proc. 1<sup>st</sup> Int. Conf. Computat. Intell. Networks (CINE)*, pp. 47–51, 2015.
- [32] P. Motsoeneng, J. Bamukunde, and S. Chowdhury, “Comparison of perturb & observe and hill climbing MPPT schemes for PV plant under cloud cover and varying load,” in *10<sup>th</sup> Int. Renewable Energy Cong. IREC*, pp. 1–6, 2019.
- [33] N. Femia, G. Petrone, G. Spagnuolo, and M. Vitelli, “Optimization of perturb and observe maximum power point tracking method,” *IEEE Trans. Power Electron.*, vol. 20, no. 4, pp. 963–973, 2005.
- [34] R. Thankakan and E. R. Samuel Nadar, “Investigation of thermoelectric generators connected in different configurations for micro-grid applications,” *Int. J. Energy Res.*, vol. 42, no. 6, pp. 2290–2301, 2018.